Princeton Plasma Physics Laboratory

PPPL- 4538

PPPL- 4538

Objectives and Layout of a High-Resolution X-ray Imaging Crystal Spectrometer for the Large Helical Device (LHD)

M. Bitter, K. Hill, D. Gates, D. Monticello, H. Neilson, A. Reiman, A.L. Roquemore,
S. Morita, M. Goto, H. Yamada, J. E. Rice

July, 2010

Prepared for the U.S. Department of Energy under Contract DE-AC02-09CH11466.

Princeton Plasma Physics Laboratory
Report Disclaimers

Full Legal Disclaimer

Trademark Disclaimer

PPPL Report Availability

Princeton Plasma Physics Laboratory:

http://www.pppl.gov/techreports.cfm

Office of Scientific and Technical Information (OSTI):

http://www.osti.gov/bridge

Related Links:

U.S. Department of Energy

Office of Scientific and Technical Information

Fusion Links

Objectives and Layout of a High-Resolution X-ray Imaging Crystal Spectrometer for the Large Helical Device (LHD)[a)]

M. Bitter,[1, b)] K. Hill,[1] D. Gates,[1] D. Monticello,[1] H. Neilson,[1] A. Reiman,[1] A. L. Roquemore,[1] S. Morita,[2] M. Goto,[2] H. Yamada,[2] J. E. Rice,[3]

[1]*Princeton Plasma Physics Laboratory, Princeton, New Jersey 08543, USA*
[2]*National Institute for Fusion Science, Toki 509-5292, Gifu, Japan*
[3]*Plasma Fusion Center, MIT, Cambridge, Massachusetts 02139-4307*

(Presented XXXXX; received XXXXX; accepted XXXXX; published online XXXXX)
(Dates appearing here are provided by the Editorial Office)

A high-resolution X-ray imaging crystal spectrometer, whose concept was tested on NSTX and Alcator C-Mod, is being designed for LHD. This instrument will record spatially resolved spectra of helium-like Ar^{16+} and provide ion temperature profiles with spatial and temporal resolutions of < 2 cm and ≥ 10 ms. The stellarator equilibrium reconstruction codes, STELLOPT and PIES, will be used for the tomographic inversion of the spectral data. The spectrometer layout and instrumental features are largely determined by the magnetic field structure of LHD.

I. INTRODUCTION

The recent development of x-ray imaging crystal spectrometers, which record spatially resolved spectra of highly charged ions of medium-Z elements from argon through tungsten, made it possible to measure profiles of the ion-temperature and profiles of the toroidal rotation velocity in tokamak plasmas for almost all experimental conditions [1-4]. By contrast, the charge exchange recombination spectroscopy [5-7], which is now widely used for the diagnosis of ion temperature profiles in tokamak plasmas, requires the injection of energetic hydrogen or deuterium beams and can therefore not be applied: (1) if as on Alcator C-Mod and ITER, the electron density and temperature are so high and the plasma dimensions so large that neutral beams cannot penetrate to the core of the plasma, (2) if as on EAST and KSTAR, which are tokamaks with superconducting magnetic field coils, the injection of a neutral beam for the purpose of ion temperature measurements cannot be maintained for the full duration of a plasma discharge of several minutes, and (3) if the injection of a neutral hydrogen beam would perturb an experimental investigation as, for instance, a study of the intrinsic plasma rotations, which occur without external momentum input, or studies of RF-heating and lower-hybrid current drive. The Large Helical Device, a stellarator of large dimensions with superconducting coils, long plasma pulses of several minutes, densities in the range from 10^{19} to 10^{20} m^{-3}, and electron temperatures up to 10 keV [8 - 10], belongs to this category of experiments and will therefore benefit from the diagnostic capabilities of an x-ray imaging crystal spectrometer that is presently being designed under a NIFS/PPPL collaboration agreement.

II. OBJECTIVES

The objectives the NIFS/PPPL collaboration are twofold: The first objective is to design and install an x-ray imaging crystal spectrometer on LHD for measurements of ion temperature profiles with spatial and temporal resolutions of < 2 cm and ≥ 10 ms, using the spectra of helium-like argon, which are already being observed on LHD with a single-chord Johann type x-ray crystal spectrometer [11, 12]. An example of a helium-like argon spectrum that was recorded from LHD with this instrument is shown in Fig. 1. This spectrum covers the wavelength range from 3.94 to 4.00 Å and consists of the main helium-like lines w, x, y, and z, and the numerous $n \geq 2$ satellites [13, 14]. Due to constraints imposed by the stellarator geometry and other experimental constraints, which are explained in the following section, the planned new x-ray imaging spectrometer will record only a small part of this spectrum, which includes the resonance line w and the associated nearby $n \geq 3$ dielectronic satellites. In addition to ion temperature profiles, which are derived from the Doppler width of the resonance line w, it will therefore also be possible to measure profiles of the electron temperature from the satellite-to-resonance-line ratios. The second objective is to

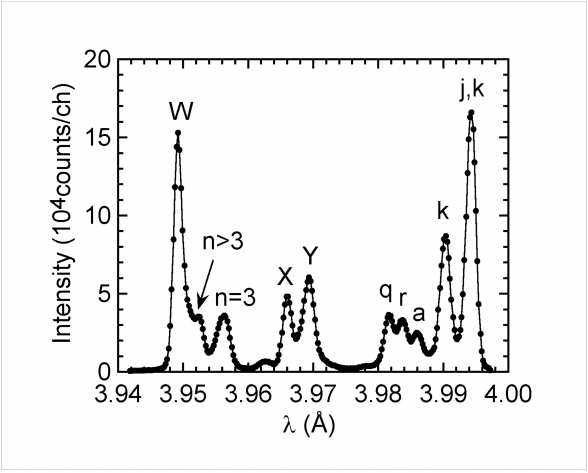

FIG. 1. He-like argon spectrum from existing Johann crystal spectrometer on LHD

[a)]Contributed paper published as part of the Proceedings of the 18th Topical Conference on High-Temperature Plasma Diagnostics, Wildwood, New Jersey, May, 2010.
[b)]Author to whom correspondence should be addressed. Electonic mail: bitter@pppl.gov

provide theoretical support for the data analysis, using the stellarator equilibrium reconstruction codes STELLOPT and PIES [15-19]. Equilibrium reconstruction is a necessary first step in doing theoretical analysis, such as transport and stability calculations. In three-dimensional equilibria, there is an issue of equilibrium flux surface loss, so that the equilibrium itself is of interest for determining the extent of pressure-driven flux surface stochastization. Equilibrium reconstruction for the W7AS stellarator indicated that, in some cases, equilibrium flux surface loss played an important role in limiting the achievable β [15, 16]. For these calculations, the STELLOPT reconstruction code [15, 17] was first used to obtain an equilibrium reconstruction assuming nested flux surfaces. The resulting equilibrium solution was then used as the starting point for the calculation with the PIES code [18, 19], which does not assume good flux surfaces, i.e. the reconstructed pressure and current profiles from the STELLOPT calculation were used in the PIES equilibrium. For the LHD data analysis, the PIES equilibrium reconstruction will be improved to use the diagnostic signals directly, and to calculate reconstructed pressure and current profiles that give an optimal fit to the diagnostic data. For this purpose, it will be desirable to have electron and ion densities, local impurity concentrations, as well as magnetic diagnostics signals, in addition to the data from the x-ray imaging crystal spectrometer. Synthetic diagnostics will be incorporated in the PIES code. Thus, the chord-integrated data from the crystal spectrometer, will be simulated by integrating over the theoretically predicted local values. The simulated data will be compared with the actual data, and the pressure and current profiles will be constructed to give a best fit to the experimental data, including those from the crystal spectrometer. As a first step, however, it will be desirable to initially use tomographically inverted data.

III. Spectrometer Layout for LHD

The complicated magnetic field configuration of LHD and the resulting peculiar shapes of the plasma cross-section require modifications of the spectrometer design, commonly used on tokamaks. As shown in Fig. 2, the spectrometer consists of a spherically bent crystal and a two-dimensional position-sensitive detector, which are arranged in a Johann configuration [20]. X-rays of a certain wavelength λ, which are emitted from the plasma, reflected by the crystal with a Bragg angle θ according to the Bragg condition, and focused to a point P in the detector plane, seem to emanate from a *sagittal* line source at B_s because of the astigmatism of a spherically bent crystal. For the preferred experimental arrangement of crystal and detector, shown in Fig. 2, this *sagittal* line source is parallel to the toroidal magnetic field. The astigmatism is then of no concern since the electron density and electron temperature and thus the x-ray emissivity are uniform along the toroidal magnetic field. Since the ray pattern is symmetric with respect to rotations about the axis OC, one obtains a one-dimensional image of the plasma on the detector, with spatial resolution perpendicular to the toroidal magnetic field. The design of an x-ray imaging crystal spectrometer for LHD is, however, complicated due to the fact that the magnetic field varies rapidly with the toroidal angle Φ, so that there are only a few locations around the torus, where the magnetic field has a predominant toroidal component. These locations are the most appropriate locations for the installation of an x-ray imaging crystal spectrometer. However, the spectrometer must still be designed in such a way that the length of the *sagittal* line source is compatible with the scale length for the magnetic field variations. As can be inferred from Fig. 2, the length of the

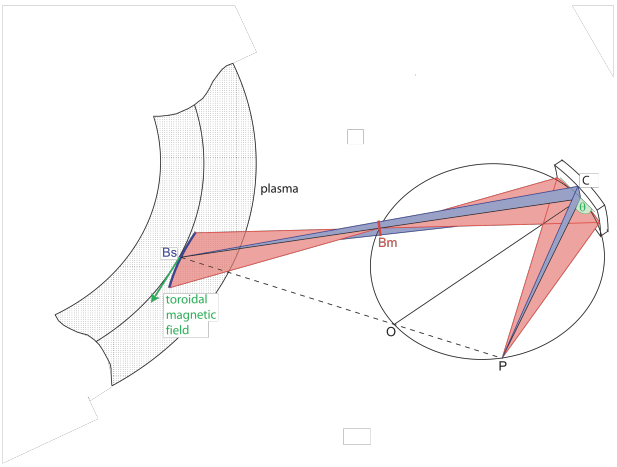

FIG. 2. Preferred arrangement of an x-ray imaging crystal spectrometer on tokamaks and stellarators

sagittal line source is determined by the width of the crystal and Bragg angle θ. The distances of the *sagittal* line source and its point-image P from the crystal are $b_s = -R \bullet \frac{\sin(\theta)}{\cos(2\theta)}$ and $p = R \bullet \sin(\theta)$, where R is the radius of curvature of the crystal. The x-ray imaging crystal spectrometer will be installed on the equatorial port, AL01-07, at the end of the LHD pump duct, where the magnetic field has a predominant toroidal component over a scale length of l_s=120 mm and where the plasma cross-section has an elliptical shape with a 1500 mm long major half axis in the equatorial plane and a 500 mm long minor half axis perpendicular to the equatorial plane - see Fig 3. The fact that the minor half axis is perpendicular to the equatorial plane has the advantage that a minimum number of detectors is needed to obtain a de-magnified one-dimensional image of the entire plasma. Port, AL01-07, is equipped with a 12 in.-diameter gate valve, which is at a distance of 19811 mm from the center of LHD. To avoid interferences with other diagnostics the crystal will be placed at a distance of 2672 mm from this gate valve. The center of the plasma is at a distance of 3750 mm from the center of LHD, so that the distance between the crystal and center of the plasma is d_{cp}=18733 mm – see Fig. 3. In order to place the *sagittal* line source as close as possible to the center of the plasma and to assure that the length of the *sagittal* line source is compatible with the scale length, l_s=120 mm, for the above-mentioned magnetic field variations, the spectrometer will be equipped with a spherically bent 110-quartz crystal with a 2d-spacing of 2d=4.91304 Å, a radius of curvature of R=5890 mm, a width w=40 mm, and height h=100 mm. Since the wavelength of the resonance line w is λ=3.9494 Å, this line will be observed at a Bragg angle of Θ=53.50°, so that b_s=16195 mm and p=4735 mm. The spatial resolutions, Δy and Δz, in the toroidal and vertical directions at the center of the plasma are $\Delta y < l_s$, and $\Delta z = h \bullet \frac{d_{cp} - b_s}{b_s} < 20mm$. These values can be improved by reducing the width and height of the crystal with an appropriate mask. The de-magnification of the one-dimensional image of the plasma in the detector plane is $\frac{p}{d_{cp}} = 0.253$, so that a 1 m high plasma can be imaged onto a PILATUS 300K-W detector system [21], which comprises three Pilatus II detector

modules and which has a total sensitive area of 254 x 335 mm^2 with 287,625 (0.172x0.172 mm^2 large) pixels. The spatial information will be displayed on the 254 mm long dimension and the wavelength on the 33.5 mm long dimension of the detector. The wavelength dispersion in the detector plane is $6.11 \bullet 10^{-4} \frac{\AA}{mm}$, so that the observed spectral range extends from 3.94 to 3.96 Å. This spectral range includes the resonance line w and the $n \geq 3$ satellites - see Fig. 1. The traces of the spectral lines in the detector plane are sections of ellipses; the major and minor half axes of the ellipse for the line w are a=7743 mm and b=5208 mm. Figure 3 shows the plasma cross-section at port AL01-07 with contours of constant magnetic flux tubes and a number of arbitrary sightlines of the x-ray imaging crystal spectrometer in the upper half of the plasma. The spacing between these sightlines at the center of the plasma is 50 mm or somewhat larger than twice the spatial resolution. Note that the whole plasma cross-section is included between the outermost sightlines (the two red lines in Fig. 3) passing through the points at $\pm$ 127 mm of the Pilatus 300K-W detector, so that the whole plasma can be observed simultaneously. (Sightlines through the lower half of the plasma are not shown only to assure visibility of the constant flux contours.) The vertical inclination of all the spectrometer sightlines is between $\pm$1.5°. The Pilatus II detector modules are based on the modern CMOS hybrid-pixel technology [21, 22]. Important features are their high neutron tolerance and high single-photon count rate capability of 2 MHz per pixel. The Pilatus II detector modules were tested for damage up to 10^{14} equivalent 1 MEV neutrons per cm^2 and have been operated on NSTX without shielding during deuterium plasma discharges with 6 MW of neutral deuterium beam injection. Under these conditions the background due to neutrons was 250 counts/s per pixel, whereas the typical number of x-ray photons/s per pixel was between 5000 and 10000 [23]. The background due to neutrons could easily be reduced by a factor of 10 with some shielding of the detectors by lead and borated polyethylene. It is, however, noteworthy that even unshielded Pilatus II detectors are not saturated under the experimental conditions on NSTX due to their high count rate capability. Based on the data from the existing crystal spectrometer on LHD, we estimate that the typical x-ray count rate for the new x-ray imaging crystal spectrometer will be about 10^4 photons/s per pixel. The layout of the spectrometer is shown in Fig. 4. The crystal housing will be connected to the 12 in. diameter gate valve on port, AL01-07, by a 3 m long vacuum pipe of varying diameter from 10 in. near the

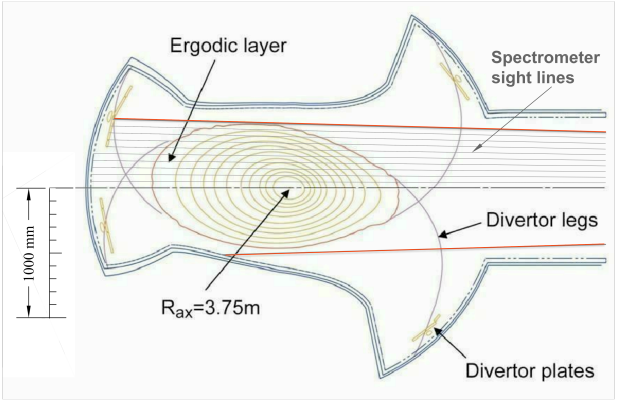

FIG. 3. Plasma cross-section with contour plots of constant magnetic flux tubes and some sightlines of the x-ray imaging crystal spectrometer

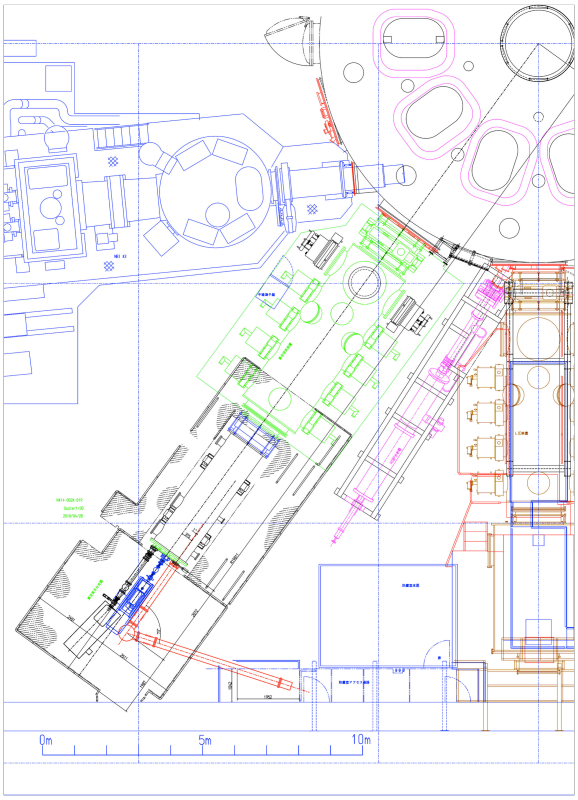

FIG. 4. Layout of x-ray imaging crystal spectrometer on port AL01-07 at the end of the LHD pump-duct

gate valve to 6 in. near the crystal housing. Similarly, the crystal and detector housings will be connected by a 5 m long vacuum pipe, whose diameter varies from 6 in. near the crystal housing to 14 in. at the location of the detector. The crystal chamber will be separated from the LHD vacuum vessel by a 75 μ thick, 3x5 in.^{2} wide, beryllium window, which will be installed on the crystal housing. The dimensions of the beryllium window, gate valve, and vacuum pipes are such that each crystal element has an unimpeded view of the whole plasma and the Pilatus 300K-W detector. The crystal chamber will be under vacuum to avoid attenuation of the 3 keV x-rays in air; and the Pilatus 300K-W detector will, therefore, be operated in vacuum: It will be turned on during LHD discharges and turned off between discharges for cooling. – The new x-ray imaging crystal spectrometer will be installed on LHD in April 2011.

Acknowledgements

This work is being supported by the US Department of Energy, Contract No. DE-AC02-09CH11466

[1]M. Bitter, K. W. Hill, B. Stratton, A. L. Roquemore, D. Mastrovito, S. G. Lee, J. G. Bak, M. K. Moon, U. W. Nam, G. Smith, J. E. Rice, P. Beiersdorfer, B. S. Fraenkel, Rev. Sci. Instrum. **75**, 3660 (2004).
[2]A. Ince-Cushman, J. E. Rice, M. Bitter, M. L. Reinke, K. W. Hill, M. F. Gu, E. Eikenberry, Ch. Broennimann, S. Scott, Y. Podpaly, S. G. Lee, and E. S. Marmar, Rev. Sci. Instrum. **79**, 10E302 (2008).
[3]J.E. Rice, A.C. Ince-Cushman, P.T. Bonoli, M.J. Greenwald, J.W. Hughes, R.R. Parker, M.L. Reinke, G.M.Wallace, C.L. Fiore, R.S. Granetz, A.E. Hubbard, J.H. Irby, E.S. Marmar, S. Shiraiwa, S.M. Wolfe, S.J. Wukitch, M. Bitter, K. Hill and J.R.Wilson, Nucl. Fusion **49**, 025004 (2009).

[4]A. Ince-Cushman, J. E. Rice, M. Reinke, M. Greenwald, G. Wallace, R. Parker, C. Fiore, J.W. Hughes, P. Bonoli, S. Shiraiwa, A. Hubbard, S. Wolfe, I. H. Hutchinson, and E. Marmar, M. Bitter, J. Wilson, and K. Hill, Phys. Rev. Lett. **102**, 035002 (2009).
[5]R. Isler, Phys. Scr. **35**, 650 (1987).
[6]R. J. Fonck, D. S. Darrow, and K. P. Jachnig, Phys. Rev. A **29**, 3288 (1984).
[7]R. Isler, Plasma Phys. Control. Fusion **36**, 171 (1994).
[8]A. Komori et al., Fusion Sci. Tech. 50, 136 (2006).
[9]H. Yamada, et al., Phys. Rev. Lett. **84**, 1216 (2000).
[10]S. Kubo, et al., J. Plasma and Fusion Research: Rapid Communications **78**, 99 (2002).
[11]S. Morita and M. Goto, Rev. Sci. Instrum. **74**. 2375 (2003).
[12]M. Goto and S. Morita, J. Plasma and Fusion Research: Regular Articles Vo. 5 S1040 (2010); *Proceedings 18th International Toki Conference (ITC18). Development of Physics and Technology of Stellarators/Heliotrons "en route to DEMO."* .
[13]L. A. Vainshtein and U. I. Safronova, At. Data Nucl. Data Tables **21**, 49 (1978); **25**, 311 (1980); *and* L. A. Vainshtein and U. I. Safronova, Lebedev, P. N., Institute of Spectroscopy, Report No. 2 (1985).
[14]TFR Group, F. Bombarda, F. Bely-Dubau, M. Cornille, J. Dubau, and M. Loulergue, Phys. Rev. A **32**, 2374 (1985).
[15]M.C. Zarnstorff *et al.*, *Proc. 20th Int. Conf. on Fusion Energy 2004, Vilamoura, Portugal, 2004* (Vienna: IAEA) CD-ROM EX/3-4.
[16]A. Reiman, M.C. Zarnstorff, D. Monticello, A. Weller, J. Geiger, et al, Nucl. Fusion **47, 572** (2007).
[17]S. P. Hirshman, D. A. Spong, J. C. Whitson, V. E. Lynch, D. B. Batchelor, B. A. Carreras, J. A. Rome, Phys Rev Letters **80,** 528 (1998).
[18]A. Reiman, and H. S. Greenside, J. Comput. Phys. **75** (1988) 423.
[19]D. Monticello, J. Johnson, A. Reiman, and P. Merkel, in *Proceedings of the Tenth International Workshop on Stellarators*, EUR-CIEMAT 30 (1995) p. 45-48.
[20]H. H. Johann, Z. Phys. **69**, 185 (1931).
[21]http://www.dectris.com/sites/pilatus300k-w.html.
[22]Ch. Broennimann, et al., J. Synchrotron Rad. **13**, 120 (2006).
[23]K. W. Hill, et al., at this conference, paper: C10658_L35

The Princeton Plasma Physics Laboratory is operated
by Princeton University under contract
with the U.S. Department of Energy.

Information Services
Princeton Plasma Physics Laboratory
P.O. Box 451
Princeton, NJ 08543

Phone: 609-243-2245
Fax: 609-243-2751
e-mail: pppl_info@pppl.gov
Internet Address: http://www.pppl.gov